Accepted by ApJ
Preprint typeset using LaTeX style emulateapj v. 11/12/01

THE THERMALLY-UNSTABLE WARM NEUTRAL MEDIUM: KEY FOR MODELING THE ISM

Ayesha Begum[1], Snežana Stanimirović[1], W. M. Goss[2], Carl Heiles[3], Anthony S. Pavkovich[1] & Patrick Hennebelle[4]
[1]University of Wisconsin, Madison, 475 N Charter St, Madison, WI 53706, [2]National Radio Astronomy Observatory, P.O. Box O, 1003 Lopezville, Socorro, NM 87801 [3]Radio Astronomy Lab, UC Berkeley, 601 Campbell Hall, Berkeley, CA 94720, [4]Laboratoire de radioastronomie, UMR 8112 du CNRS, 24 rue Lhomond, 75231 Paris, France
begum@astro.wisc.edu, sstanimi@astro.wisc.edu
Accepted by ApJ

ABSTRACT

We present 21-cm absorption measurements towards 12 radio continuum sources with previously identified thermally-unstable warm neutral medium (WNM). These observations were obtained with the Expanded Very Large Array (EVLA) and were complemented with the HI emission spectra obtained with the Arecibo Observatory. Out of 12 sources, HI absorption was detected along 5 lines of sight (seven new absorption features in total), resulting in a detection rate of ~ 42 %. While our observations are sensitive to the WNM with a spin temperature $T_s < 3000$ K, we detected only two wide absorption lines with $T_s = 400 - 900$ K. These temperatures lie above the range allowed for the cold neutral medium (CNM) by the thermal equilbrium models and signify the thermally unstable WNM. Several absorption features have an optical depth of only a few $\times 10^{-3}$. While this is close or lower than what is theoretically expected for the CNM, we show that these weak lines are important for constraining the fraction of the thermally unstable WNM. Our observations demonstrate that, for the first time, high bandpass stability can be achieved with the VLA, allowing detection of absorption lines with a peak optical depth of $\sim 10^{-3}$.

Subject headings: ISM: clouds — ISM: structure — radio lines: ISM

1. INTRODUCTION

The diffuse neutral interstellar medium (ISM) is known to exist in two flavors: the cold neutral medium (CNM) and the warm neutral medium (WNM). Traditionally, the CNM and WNM are understood as being two thermal equilibrium states of the neutral ISM with temperature of $40 - 200$ K and $\sim$ 8000 K (Field et al. 1969; McKee & Ostriker 1977; Wolfire et al. 2003). In addition, for the CNM the spin temperature, $\mathrm{T_s} \sim \mathrm{T_k}$ is expected from theoretical considerations. The situation is more complicated in the case of the WNM and T_s could be lower than T_k (Liszt 2001). Observationally, the CNM is easily studied with the 21-cm line absorption. While the CNM properties have been measured extensively, only three direct measurements of the WNM spin temperature exist to date (Kanekar et al. 2003; Dwarakanath et al. 2002; Carilli et al. 1998). The main reason for this observational paucity is the low optical depth of the WNM, $\tau \lesssim 10^{-3}$, which creates a need for very sensitive radio instruments. Properties of the WNM are traditionally indirectly inferred only through HI emission line profiles. Out of all ISM phases, the WNM is the least understood; yet it seems to hold the key for constraining ISM models and the formation of CNM clouds.

The theoretical and numerical models of the ISM take into account heating and cooling processes and try to reproduce the observed physical properties of the CNM and the WNM. These properties include temperature distribution, column density probability density functions (PDFs), the gas fraction in each phase, and even profiles of emission and absorption spectra. McKee & Ostriker (1977), and similarly Wolfire et al. (2003), predict that most of the WNM, which in their model envelopes the CNM, should be in thermal equilibrium and comprise only about 4% of the total column density. However, observers have traditionally found a much higher fraction for the WNM.

In addition, a significant fraction of the WNM could be thermally unstable. Using a statistically meaningful sample and the Arecibo radio telescope, Heiles & Troland (2003; HT03) found that 48% of the WNM in their survey was in the thermally unstable phase, with kinetic temperatures in the range of $500 - 5000$ K. The HT03 results question the meaning of a two-phase neutral medium and have triggered substantial numerical studies. Numerical models of the ISM which include turbulence easily find thermally unstable gas and lead to the conclusion that dynamical processes overshadow the microscopic ones in determining gas temperature. Macroscopical processes are hard to calculate theoretically because they depend on many forms of energy input (HT03). As a result, the predicted column density fraction of the thermally unstable gas varies wildly; from very large values strongly dependent on the SN rate, as in Mac Low et al. (2005), to $\sim 30\%$ in Hennebelle et al. (2007).

However, the estimated fraction of the thermally unstable WNM in HT03 could be significantly biased by the low sensitivity of this survey. In many of the observed directions (16 out of 79 in this survey) the CNM was not detected at all. In addition, there were many cases where relatively narrow WNM components (based on Gaussian fits) were found without corresponding CNM features. These WNM components often implied kinetic temperatures of 2000-3000 K and are typical representatives of the thermally unstable phase. As discussed in HT03, one possibility is that these lines of sight trace special conditions where the CNM was destroyed in some way

TABLE 1
EVLA OBSERVATIONS

Source	RA(J2000) (Deg)	Dec (J2000) (Deg)	S_{1420} (Jy)	rms (mJy)	τ_{rms}	Synthesized beam (arcsec^2)	Time (hrs)
J0022+002	00:22:25.4	+00:14:56	3.05	4.4	0.0014	14.0 × 10.0	5.0
J0025-260	00:25:49.2	−26:02:12	8.81	7.5	0.0009	17.0 × 12.0	1.0
P0347+05*	03:49:46.7	+05:51:38	1.96	4.7	0.0024	14.0 × 9.0	5.0
3C234*	10:01:49.0	+28:47:12	2.12	8.0	0.0038	13.0 × 9.0	2.0
3C236	10:06:01.8	+34:54:12	3.22	4.8	0.0015	13.0 × 9.0	5.0
3C263.1	11:46:19.9	+22:04:10	3.23	3.8	0.0011	13.0 ×9.0	5.0
3C273*	12:29:06.4	+02:03:05	32.7	10.0	0.0003	14.0×9.0	1.0
3C287	13:30:37.7	+25:09:10	6.69	6.0	0.0009	13.0×9.0	1.0
3C286	13:31:08.3	+30:30:33	16.0	3.2	0.0002	13.0 × 12.0	10.0
J1613+324	16:13:41.1	+34:12:47	4.40	5.0	0.0011	12.5 × 9.0	2.0
J1634+627	16:34:33.8	+62:45:35	5.14	5.8	0.0011	13.0 × 10.0	2.0
J1635+381	16:35:15.5	+38:08:04	2.52	4.0	0.0016	13.4 × 8.6	5.0

* The continuum source is resolved with the EVLA observations.

(SNe etc). However, the integration time of only 15 min per source resulted in a typical optical depth sensitivity of $\sim 10^{-2}$. Stanimirović & Heiles (2005) showed that with longer Arecibo integrations, weak absorption lines, with $\Delta\tau \sim 10^{-3}$, are easily detected. These weak absorption lines play an important role in the fitting of HI emission spectra and the derivation of the spin temperature. If commonly found in observations, the weak absorption lines would result in a decrease of the estimated fraction of the thermally unstable WNM.

In this paper we report the results of deep HI absorption observations with the Expanded VLA (EVLA) in the directions of thermally-unstable WNM. The main goal of this project was to test the feasibility of sensitive HI absorption measurements with a peak optical depth $\tau \sim$ a few $\times 10^{-3}$ with the EVLA. In two independent pilot projects carried out with the VLA in 2006 & 2009, we observed a sample of 12 continuum sources. The sources were chosen from the previous emission/absorption surveys of HT03 and Mohan et al. (2004). We specifically focused on lines of sight where previous observations indicated the existence of the thermally-unstable WNM with a kinetic temperature < 5000 K. All continuum sources in our sample are at high Galactic latitudes i.e. $|b| > 40°$, to avoid complicated CNM profiles.

The structure of this paper is organized in the following way. Section 2 summarizes the EVLA observations and the data reduction. Our results are presented in Section 3 and discussed in Section 4. We summarize our findings in Section 5.

2. OBSERVATIONS AND DATA PROCESSING

We observed 3C286 in April 2008 with the VLA during the configuration move CnB→C and using 14 EVLA antennas. HI absorption observations of additional 11 sources were carried out in May 2009 during the B→C configuration move and using 20 EVLA antennas.

In Table 1 we list coordinates and the 21-cm flux density of all observed sources, as well as a few observational details. Column (1) gives the source name, columns (2) and (3) the source RA and Dec in J2000 coordinates, column (4) the flux density at 21 cm determined from our EVLA observations, column (5) the rms noise in each line channel in mJy, column (6) the rms noise per channel in the optical depth units, column (7) the synthesized beam size, and column (8) the total on-source integration time.

For all observations we used a bandwidth of 1.56 MHz, centered at the frequency of the 21-cm HI line, with 256 spectral channels. The resulting velocity resolution is 1.56 km s^{-1}. For absolute flux density calibration we observed sources 3C286 and 3C48. Since most of our the sources are bright, amplitude and phase calibrations of the antennas were carried out through self-calibration. The bandpass calibration was obtained through frequency switching on the source itself. For this purpose, each 15 minute"on-line" scan was sandwiched between two 7 minute "off-line" scans. The off-line scans were offset in frequency from the on-line scans by 1.56 MHz and were not affected by contamination due to Galactic HI. This observing strategy provided accurate bandpasses. To test the quality of our bandpasses, we used one of the "off-line" scans as a bandpass for the other "off-line" scan. This resulted in a flat spectrum with a rms noise of 2×10^{-3} for weak sources such as 3C263.1, and $\sim 10^{-4}$ for stronger sources.

The visibility data was analyzed using the Astronomical Image Processing System (AIPS). For each source, line-free channels were averaged to construct a single continuum channel. The amplitude and phase antenna solutions were obtained through normal and self calibration of this continuum channel and then transferred to the spectral line visibility data. The calibrated and bandpass corrected spectral line data was used for further analysis. The continuum was removed using the AIPS task UVLSF by performing a polynomial fit to the visibilities in the line-free channels and subtracting it from the source visibilities in all the spectral channels. For most sources a first or a second-order fit was used to remove the continuum. In the case of two sources, 3C286 and J1635+381, a 3rd-order polynomial was required to obtain a flat baseline. Before continuum subtraction the spectrum from each source was carefully inspected to select line-free channels. The continuum subtracted visibilities were used to make spectral cubes of the HI absorption in the direction of each source. The spectral cubes were CLEANed using the AIPS task

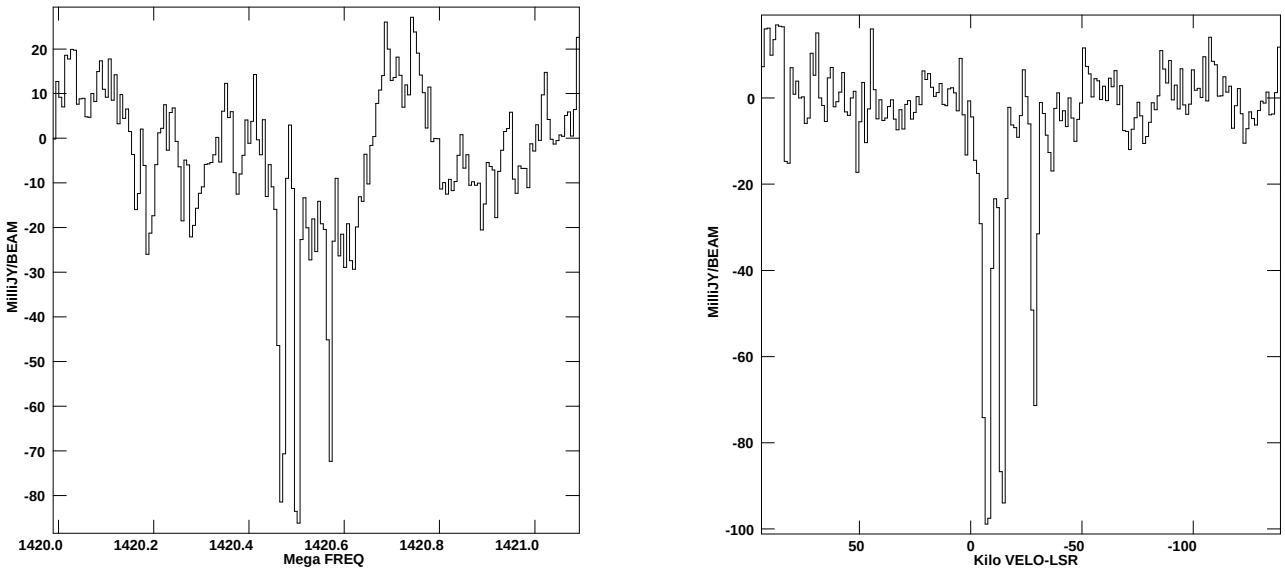

FIG. 1.— The HI absorption spectrum in the direction of 3C286 obtained with VLA antennas only (left), and the EVLA antennas only (right). The bandpass stability is largely improved with the use of EVLA antennas and allowed a clear detection of spectral lines with very low optical depth. The deepest absorption feature in the right-hand figure corresponds to $\tau \sim 6 \times 10^{-3}$.

TABLE 2
THE GAUSSIAN PARAMETERS FROM THE FIT OF THE EVLA ABSORPTION SPECTRA

Source	$\tau_{\rm peak}$	$V_{\rm LSR}$ (kms^{-1})	FWHM (kms^{-1})	$T_{\rm spin}$ (K)	$T_{k,max}$ (K)	N(HI)$_{\rm CNM}$ (10^{20} cm^{-2})	N(HI)$^{\rm Upper}_{\rm CNM}$ (10^{20} cm^{-2})
J0022+002	0.0074 ± 0.0011	1.58	7.92	421 ± 46	1358	0.477 ± 0.158	1.54
J0022+002	0.0132 ± 0.0018	−5.51	4.18	137 ± 33	377	0.147 ± 0.048	0.40
P0347+05	0.9564 ± 0.0199	8.09	3.18	61 ± 5	219	3.609 ± 0.113	12.97
P0347+05	0.2972 ± 0.0168	9.75	7.31	148 ± 3	1155	6.266 ± 0.398	48.89
P0347+05	0.0459 ± 0.0046	−0.47	4.05	175 ± 12	355	0.632 ± 0.112	1.29
3C263.1	0.0252 ± 0.0024	−54.12	2.22	25 ± 10	107	0.027 ± 0.004	0.12
3C273	0.0177 ± 0.0016	−6.28	2.59	71 ± 5	146	0.063 ± 0.009	0.13
3C273	0.0036 ± 0.0017	−5.89	7.77	910 ± 19	1307	0.516 ± 0.258	0.74
3C286	0.0046 ± 0.0004	−28.79	2.66	95 ± 16	153	0.024 ± 0.005	0.04
3C286	0.0067 ± 0.0004	−14.26	2.58	39 ± 12	144	0.013 ± 0.004	0.05
3C286	0.0064 ± 0.0003	−7.39	4.49	26 ± 18	437	0.015 ± 0.010	0.25

IMAGR.

The bandpass stability was greatly improved in the case of the upgraded VLA antennas. Figure 1 shows the HI absorption spectrum in the direction of 3C286, obtained using the VLA antennas only (left) and the EVLA antennas only (right). The improved bandpass stability allowed a clear detection of spectral lines with a low optical depth of a few $\times 10^{-3}$. Hence, for all sources, only the EVLA antennas were used to produce the final HI absorption spectra.

In order to estimate the spin temperature of the detected HI absorption components, the EVLA absorption profiles were complemented by the Arecibo HI emission profiles with an angular resolution of 3.5 arcmin (HT03). The emission spectra for all sources except 3C286 and J0022+002 were obtained from HT03. Since the source J0022+002 was not observed by HT03, its emission spectrum was kindly provided to us by Lou Nigra. This spectrum was also obtained with the Arecibo telescope using exactly the same observing technique as in HT03. In the case of 3C286, the HT03 emission spectrum was very noisy and we used the Arecibo emission spectrum from Stanimirović & Heiles (2005).

3. RESULTS

We have observed a total of 12 sources and detected HI absorption in five directions: 3C286, J0022+002, 3C263.1, P0347+05, and 3C273. This results in a detection rate of $\sim$ 42% for our experiment. Several detected absorption features have a peak optical depth of only few $\times 10^{-3}$. Therefore, our pilot studies successfully demonstrate the suitability of the EVLA for sensitive absorption measurements.

Figures 2−4 show HI emission and absorption spectra for the sources with detected HI absorption. We have applied the method of HT03 to estimate the spin temperature and the HI column density of the absorbing CNM, assuming that the CNM contributes to both HI absorption and emission spectra while the WNM contributes only to the HI emission spectrum. The technique is based on the Gaussian decomposition of both absorption and emission spectra, and it takes into account the fact that a certain fraction of the WNM gas may be located in front of the CNM clouds, resulting in only a portion of the WNM being absorbed by the CNM.

The results of our Gaussian decomposition are overplotted in Figures 2−4. Three panels are shown for each source. The top panel shows the Arecibo HI emission spectrum and the separate contributions from the CNM and WNM to the HI brightness temperature are shown with different lines; the final (simultaneous) fit to the spectrum is also overlayed. In the middle panel the EVLA HI absorption spectrum fitted with individual Gaussian components is shown. In the bottom panel we show the residuals of the absorption spectrum after the fitting process. For each source the residual spectrum looks random and demonstrates that the fit is perfect at the present level of the signal-to-noise ratio and that the Gaussian representation of CNM components is valid. The residual spectrum for each source was smoothed to various coarser velocity resolutions, up to $\sim$ 25.0 kms^{-1}, to search for additional broad absorption; no new components were detected.

Table 2 shows the best fitted CNM parameters. Column (1) gives the source name, column (2) the peak optical depth ($\tau_{\rm peak}$) of the CNM component along with the errorbar, column (3) the LSR velocity of the component in km s^{-1}, column (4) the full width at half maximum (FWHM) of the absorption component in km s^{-1}, and column (5) the spin temperature $T_{\rm spin}$ along with its errorbar, in Kelvin. In column (6) we list $T_{k,max}$, the maximum kinetic temperature in the case of no non-thermal broadening. Column (7) gives the HI column density associated with the CNM component along with its errorbar, in units of 10^{20} cm^{-2}, and column (8) the upper limit on the CNM HI column density, N(HI)$^{upper}_{CNM}$, also in units of 10^{20} cm^{-2}. To derive N(HI)$^{upper}_{CNM}$ we used used $T_{k,max}$ instead of $T_{\rm spin}$.

Table 3 shows the best fit WNM components for each source. Column (1) gives the source name, column (2) the LSR velocity of the WNM component in km s^{-1}, column (3) the FWHM in km s^{-1}, and column (4) the maximum kinetic temperature $T_{k,max}$ in Kelvin. We discuss the individual sources with HI absorption detections in the following sections.

For sources with no HI absorption detection, we estimated limits on the CNM column density and the CNM fraction along each line of sight. The CNM fraction is defined as the ratio of the CNM column density to the total HI column density along the line of sight. Table 4 shows the 3σ limit on the peak optical depth, the CNM column density, and the CNM fraction for sources without a detection of HI absorption.

3.1. *J0022+002 (Figures 2, left)*

No HI absorption was detected in the direction of J0022+002 by Mohan et al. (2004), whereas our more sensitive EVLA observations detected two absorption features. One of the absorption features is weak and wide with $\tau_{\rm peak} \sim 7 \times 10^{-3}$ and FWHM $\sim$ 8 km s^{-1}. While T$_{k,max}$ $\sim$ 1350 K, our estimated T$_{\rm spin}$ $\sim$ 420 K. This component is likely to trace the WNM seen in absorption. However, its temperature of 420 K is significantly lower than the expected 5000-8000 K and corresponds to the thermally unstable gas.

By fitting Gaussian functions to the emission profile alone, Mohan et al. (2004) found 5 emission components, with two components; having excitation temperatures corresponding to the thermally unstable regime. Our best solution results in two emission components, with one component having $T_k < 1500$ K and corresponding to the thermally unstable WNM. The total CNM column density along the line of sight of J0022+002 is $\sim 6 \times 10^{19}$ cm^{-2}, whereas the total WNM column density is $\sim 2\times10^{20}$ cm^{-2}; i.e the total CNM fraction is $\sim$30 %.

3.2. *P0347+05 (Figures 2, right)*

In addition to the main absorption component at a velocity of $\sim$ 8 km s^{-1}, HT03 found a narrow emission feature around V$_{\rm LSR}$ $\sim$ 0 km s^{-1} without corresponding absorption. This resulted in a thermally unstable WNM component. Figure 2 shows the EVLA absorption spectrum for this source: our detection of an additional absorption feature at -0.5 km s^{-1} results in the best-fit solution without any thermally-unstable WNM. As discussed in the introduction, this clearly demonstrates that weak

TABLE 3
THE GAUSSIAN PARAMETERS FROM THE FIT OF THE EMISSION SPECTRA

Source	V_{LSR} (kms^{-1})	FWHM (kms^{-1})	$T_{k,max}$ (10^3) K
J0022+002	−2.28	22.39	108.5
J0022+002	−4.66	8.41	1.5
P0347+05	4.95	17.33	6.5
3C263.1	−44.22	37.08	29.8
3C263.1	−39.09	8.37	1.5
3C263.1	−7.04	20.04	8.7
3C273	24.92	23.71	12.1
3C273	−15.56	35.49	27.2
3C286	−5.92	50.19	54.5
3C286	−6.08	11.35	2.8
3C286	−26.45	22.15	10.6

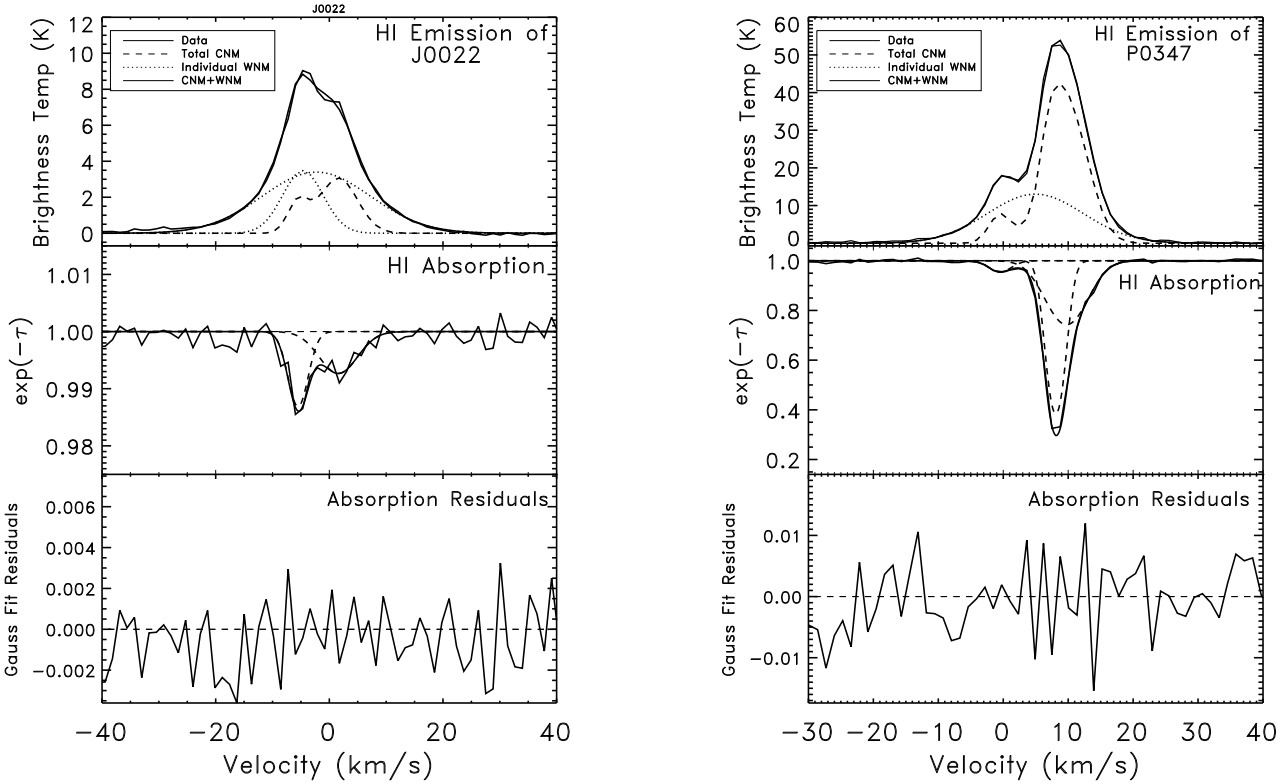

FIG. 2.— The HI emission and absorption spectra for J0022+002 (*Left*) and P0347+05 (*Right*). The top panel shows the Arecibo emission spectrum. The separate contributions from the CNM and WNM to the HI emission profile are shown with dashed and dotted lines, respectively, while the final, simultaneous fit is shown with the thick solid line. The middle panels shows the EVLA HI absorption spectrum. The fitted Gaussian functions are shown as dashed lines. The bottom panel shows the residuals of the absorption profile after the fitting procedure.

absorption lines can have a significant effect on the estimated fraction of the thermally unstable WNM. One of the detected absorption features at $V_{LSR} \sim 10$ kms^{-1} is wide and results in $T_{k,max}$ ∼1155 K, but with $T_{spin} \sim 150$ K. From Table 2&3, the total CNM fraction along the line of sight of P0347+05 is 69%.

3.3. *3C263.1 (Figure 3, left)*

We detected a narrow HI absorption component towards 3C263.1 at $V_{LSR} \sim -54.0$ kms^{-1}. HT03 did not detect any HI absorption in the direction of this source; their best fit to the emission/absorption profiles resulted in four emission components, with three components having $T_{k,max}$ corresponding to the thermally unstable WNM. From our simultaneous fitting of emission and absorption profiles, we find that the narrow emission feature corresponding to the HI absorption can be reproduced by the CNM alone without the need for a thermally-unstable WNM component. Again, the detection of weak absorption lines seems to decrease the fraction of the thermally unstable WNM. Our best-fit solution results in only one thermally unstable WNM component with $T_{k,max} < 1500$ K, while HT03 had three.

The spin temperature for the absorption component for 3C263.1 is only ∼ 30 K and is not well constrained by our method. The resulting CNM HI column density, proportional to this temperature, is very low i.e 3×10^{18} cm^{-2}. The total WNM column density in this direction is 1.6 $\times 10^{20}$ cm^{-2}, meaning that the CNM comprises only ∼ 2 % of total HI column density.

3.4. *3C273 (Figure 3, right)*

Dwarakanath et al. (2002) obtained very deep observations with the Westerbork radio telescope (WSRT) of 3C273 and detected four HI absorption components. We detected only two absorption components. The two addition components lie at the edge of our bandpass, hence they were not detected by the EVLA due to the lack of sensitivity. The two absorption components detected by the EVLA are in good agreement with Dwarakanath et al. (2002).

Figure 3 shows our emission/absorption profiles in the direction of 3C273. The HI emission profile shows three features; the HI absorption only corresponds to the narrowest emission component. Using the HT03 method we find that the narrow emission feature can be reproduced by the CNM alone with a temperature of ∼ 70 K. The HI in absorption has a narrow and a wide component. The wide component has a FWHM ∼ 8 kms^{-1} and $\tau_{peak} \sim 3 \times 10^{-3}$. The corresponding $T_{spin} = 900$ K and suggests a thermally-unstable WNM. From Table 2 & 3, the total CNM column density along the line of sight of 3C273 is ∼30 %. No HI absorption is detected corresponding to the two additional emission peaks. This places the 3σ upper limit on their spin temperature of 1665 K and 900 K, respectively.

3.5. *3C286 (Figure 4)*

HT03 detected two emission components in the direction of 3C286 but no HI absorption. Stanimirović & Heiles (2005) using Arecibo and Braun & Kanekar (2005) using the WSRT detected three weak HI absorption features through much longer integration times. As shown in Figure 4, the EVLA absorption spectrum shows three distinct features in good agreement with the Arecibo and WSRT detections. All three absorption features are weak, with $\tau_{peak} = (4-6) \times 10^{-3}$. From our best-fit solutions to the emission and absorption spectra, we find that two out of three absorption components have a very small contribution to the HI emission profiles and their T_{spin} is not well constrained. The spin temperature of these components are likely to be low, ∼ 30 K. In addition, their HI column densities are also small, a few $\times 10^{18}$ cm^{-2}. We find that the total CNM column density in the direction of this source is 5.2×10^{18} cm^{-2}, whereas the total WNM column density is 1.2×10^{20} cm^{-2}. The CNM comprises only 4% of total HI column density. Our best-fit solution results in three emission components; with only one having $T_{k,max} < 2800$ K and indicating the presence of thermally unstable gas.

3.6. *Effect of stray radiation*

The emission measurements from single dish telescopes could suffer from stray radiation entering through the sidelobes of the telescope beam. This could result in weak emission line wings and therefore affect the estimated spin temperature. To check the reliability of our temperature estimates, we compared Arecibo emission spectra with the corresponding spectra from the LAB (Leiden-Argentine-Bonn) Galactic HI survey (Kalberla et al. 2005), where the stray radiation correction has been carefully done.

We find that the Arecibo emission spectra for J0022+002, P0347+05 and 3C263.1 match well with the LAB spectra. This suggests that the Arecibo data for these sources are not effected by stray radiation and that our estimates of spin temperatures are robust. On the other hand, the Arecibo spectra for 3C273 and 3C286 show deviations from the LAB spectra. In the case of 3C273, the emission feature at ∼ 25 km s^{-1} is stronger in the Arecibo data compared to the LAB spectrum, whereas the Arecibo spectrum for 3C286 shows a faint velocity tail at ∼ 20 km s^{-1} which is not seen in the LAB stray-radiation corrected data. To check how these differences affect our estimate of T_{spin}, we repeated the Gaussian fitting analysis using the LAB emission spectra for 3C273 and 3C286. For both sources, we find that the best T_{spin} solutions derived using the LAB spectrum are consistent with the Arecibo results within the error-bars. For 3C273, the number of thermally stable/unstable WNM components is consistent with the Arecibo results. However, for 3C286, the best-fit solution using the LAB data results in three WNM components, with two being in the thermally unstable regime, as compared to only one thermally unstable WNM component when using the Arecibo data.

We conclude that majority of our sources are not effected by stray radiation and that the spin temperature derivation is robust.

4. DISCUSSION AND CONCLUSIONS

As mentioned in the previous section, we detected three wide absorption features in the direction of J0022+002, P0347+05 and 3C273, with a velocity FWHM of 7-8 km s^{-1}, and corresponding $T_{k,max}$ of 1100-1400 K. For two of these sources, our best-fit solution resulted in $T_{spin} > 400$

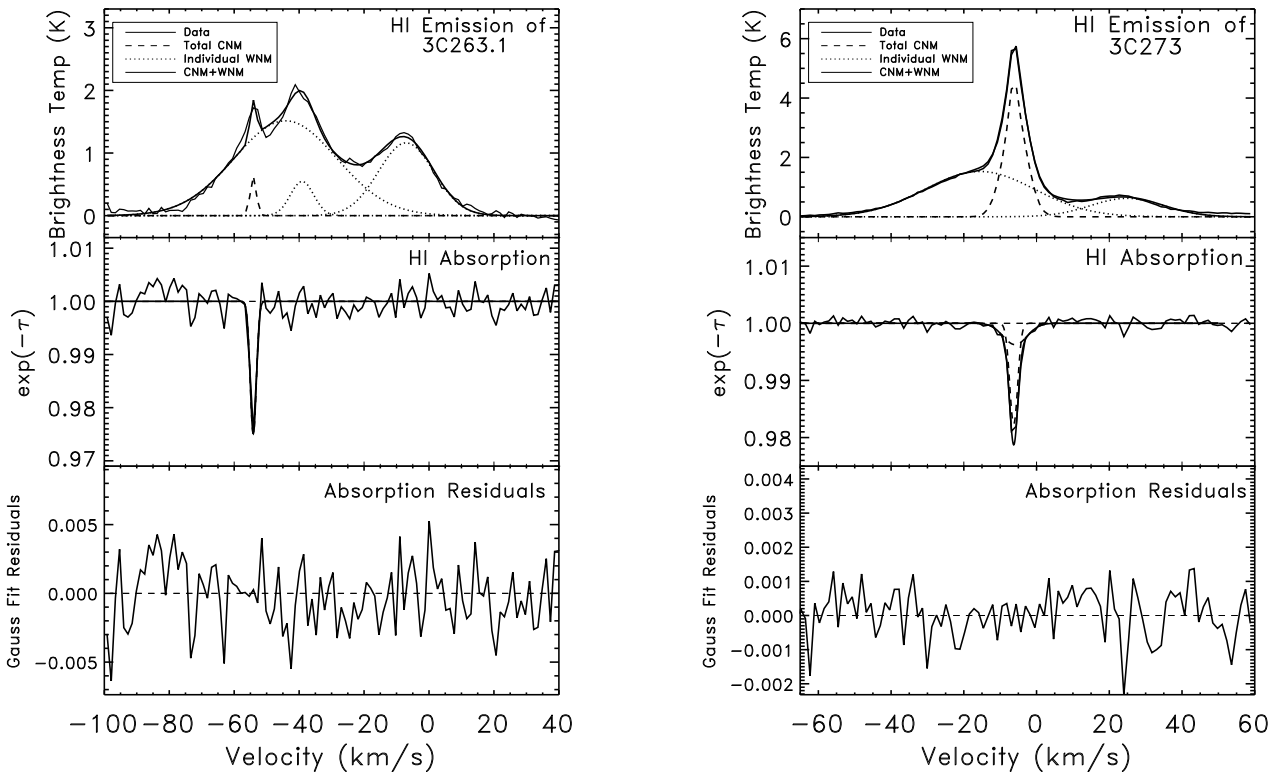

FIG. 3.— The HI emission and absorption spectra for 3C263.1 (*Left*) and 3C273 (*Right*). The top panel shows the Arecibo emission spectrum. The separate contributions from the CNM and WNM to the HI emission profile are shown with dashed and dotted lines, respectively, while the final, simultaneous fit is shown with the thick solid line. The middle panels shows the EVLA HI absorption spectrum. The fitted Gaussian functions are shown as dashed lines. The bottom panel shows the residuals of the absorption profile after the fitting procedure.

TABLE 4
LIMITS ON NON DETECTIONS

Source	$\tau_{\rm peak}$	N(HI)$^a_{\rm CNM}$ (10^{20} cm^{-2})	CNM Fraction^b (%)
J0025-260	< 0.0027	< 0.016	< 1.2
3C234	< 0.0114	< 0.066	< 4.1
3C236	< 0.0045	< 0.026	< 2.2
3C287	< 0.0027	< 0.016	< 1.4
J1613+324	< 0.0033	< 0.019	< 1.6
J1634+627	< 0.0033	< 0.019	< 1.2
J1635+381	< 0.0048	< 0.028	< 1.5

[a] N(HI)$_{\rm CNM}$ was derived assuming $T_{\rm spin}$=100 K and FWHM=3 km s^{-1}.
[b] The total HI column density was provided by HT03 and Mohan et al. (2004).

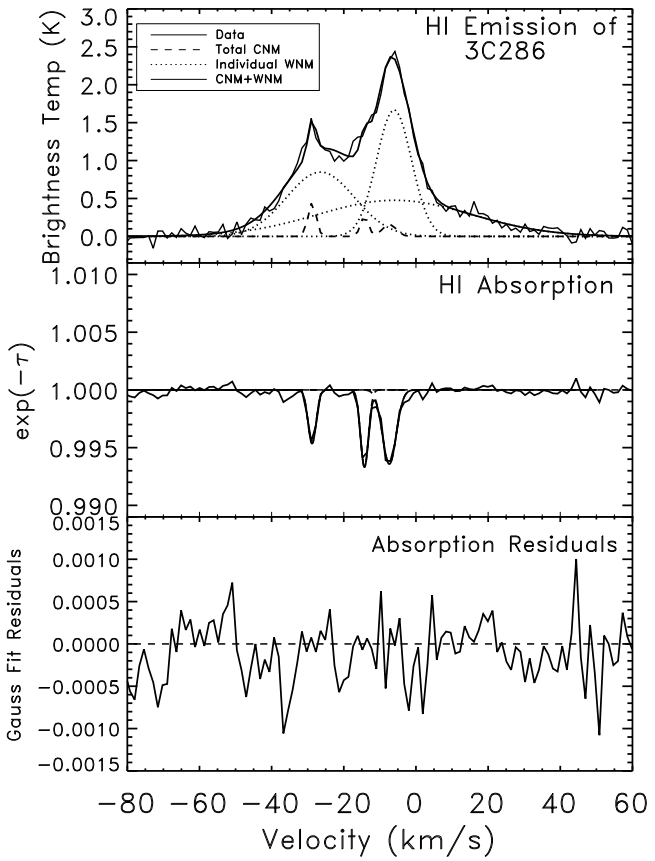

FIG. 4.— The emission and absorption spectra for 3C286. The top panel shows the Arecibo emission spectrum. The separate contributions from the CNM and WNM to the HI emission profile are shown with dashed and dotted lines, respectively, while the final, simultaneous fit is shown with the thick solid line. The middle panels shows the EVLA HI absorption spectrum. The fitted Gaussian functions are shown as dashed lines. The bottom panel shows the residuals of the absorption profile after the fitting procedure.

K. These temperatures lie above the temperature range theoretically allowed for the CNM (Wolfire et al 2003) and therefore signify the presence of thermally unstable WNM gas with a temperature $\lesssim$ 5000 K (Wolfire et al. 2003). An alternative explanation could be that these broad absorption features represent a blending of several narrow CNM absorption components. Our current velocity resolution of 1.6 km s^{-1} does not allow us to dismiss this possibility. Future EVLA observations with the WIDAR correlator will yeild a higher velocity resolution and will allow us to address this question.

The majority of detected absorption lines (8 out of 11) in this study have a velocity FWHM $<$ 5 km s^{-1} and the corresponding T$_{k,max}$ $<$ 500 K. While the 3-σ sensitivity of our observations was good enough to detect a typical WNM ($\sim 10^{20}$ cm^{-2}, HT03) in absorption with T$_s$ $\lesssim$3000 K and a FWHM $<$ 12 km s^{-1}, only two broad WNM components were detected. Both of these detections have a FWHM $\sim$ 8 km s^{-1} and T$_s$ $<$1000 K. This could be an indication that the WNM with a temperature $<$ 3000 K is not as abundant as indicated previously by indirect observations (e.g. HT03). In addition, as we clearly demonstrated in the case of P0347, the detection of weak HI absorption lines can decrease the number of thermally unstable WNM components. For the five sources with EVLA HI absorption detections, previous emission/absorption surveys (HT03 and Mohan et al. (2004)) found seven thermally unstable WNM components. Our best-fit solutions resulted in five thermally unstable components (three seen in emission and two in absorption). If applied globally, this would decrease the fraction of thermally unstable WNM components from HT03's $\sim$ 39% to $\lesssim$ 27%. We note, however, that our conclusion is based on a small number statistics and that larger and more sensitive emission/absorption surveys are required to determine the fraction of the thermally unstable WNM in a statistically significant manner.

In several cases (e.g. 3C286 and 3C263.1) we detected absorption lines which have a low optical depth and a narrow line-width which result in a low CNM column density N(HI)$_{\rm CNM}$ $< 5 \times 10^{18}$ cm^{-2}. This is significantly lower than the column density of typical CNM clouds, N$_{HI}$ $\sim 10^{20}$ cm^{-2} (Dickey et al. 1978; Heiles & Troland 2003; Dickey et al. 2003), and is close to the lowest theoretical expectations for the CNM (McKee & Ostriker 1977). In addition, in these directions the CNM comprises only 2$-$4% of the total HI column density. Sources without detected HI absorption also suggest a very low CNM fraction (Table 4). This suggests, as also pointed out by Stanimirovic, Heiles, & Kanekar (2007), that the low column density CNM population may be quite abundant in the ISM. While such small column densities and CNM fractions are hard to explain by thermal equilibrium ISM models, they may be illuminating the tail-end of the CNM population produced by dynamic and turbulent ISM processes.

5. SUMMARY

In order to access the feasibility of sensitive HI absorption observations with the EVLA, we observed a sample of 12 continuum sources, primarily along the lines of sight which have indicated the existence of the thermally-unstable WNM (T$<$ 5000 K) in previous emission/absorption surveys (Heiles & Troland 2003; Mohan et al. 2004). The results from this pilot study are as follows.

• For all, except three sources in our sample, we could achieve the expected optical depth sensitivity of $\sim 10^{-3}$. The remaining three sources were resolved with the EVLA; yielding a much lower peak flux density, hence an optical depth sensitivity $\sim 2-3$ times higher than the expected value.

• Out of 12 sources observed with the EVLA, we detected HI absorption in the direction of 5 sources; a detection rate of $\sim$42 % for our experiment. Seven new absorption features, previously undetected in the emission/absorption surveys of Heiles & Troland (2003) and Mohan et al. (2004), were detected in the direction of these 5 sources.

• In the case of several sources e.g. 3C273, P0347+05 and J0022+002, we detected wide HI absorption lines (FWHM $\sim 7-8$ km s^{-1}) resulting in T$_{k,max}$ $<$ 1500 K. These lines likely trace the thermally unstable WNM seen in absorption.

• Several detected absorption features have a peak optical depth of only a $\sim$ few $\times 10^{-3}$ and trace the tail-end of the CNM population. As we demonstrated, these weak HI absorption lines play an important role in estimating temperature of the WNM and can decrease the indirectly suggested fraction of the thermally unstable WNM.

• We have successfully demonstrated the suitability of the EVLA for future sensitive absorption measurements.

The National Radio Astronomy Observatory (NRAO) is a facility of the National Science Foundation operated under cooperative agreement by Associated Universities, Inc. The Arecibo Observatory is part of the National Astronomy and Ionosphere Center, which is operated by Cornell University under a cooperative agreement with the National Science Foundation. We thank greatly Lou Nigra (UW-Madison) for kindly obtaining the Arecibo HI emission spectrum for one of our sources. SS acknowledges support by the Research Corporation for Science Advancement.

REFERENCES

Braun, R., & Kanekar, N. 2005, A&A, 436, L53
Carilli, C. L., Dwarakanath, K. S., & Goss, W. M. 1998, ApJ, 502, 79
Dickey, J. M., McClure-Griffiths, N. M. Gaensler, B. M., & Green, A. J. 2003, ApJ, 585, 801
Dickey, J. M., Terzian, Y., & Salpeter, E. E. 1978, ApJS, 36, 77
Dwarakanath, K. S., Carilli, C. L., & Goss, W. M. 2002, ApJ, 567, 940
Field, G. B., Goldsmith, D. W., & Habing, H. J. 1969, ApJ, 155, L149
Hennebelle, P., Audit, E, & Miville-Deschenes, M. A. 2007, A&A, 465, 445
Heiles, C., & Troland, T. H. 2003, ApJS, 145, 329
Kanekar, N., Subrahmanyan, R., Chengalur, J. N., & Safouris, V. 2003, MNRAS, 346, 57L
Kalberla, P. M. W., Burton, W. B., Hartmann, D., Arnal, E. M., Bajaja, E., Morras, R., & Poppel, W. G. L. 2005, A&A, 440, 775

Liszt, H. 2001, A&A, 371, 698
Mac Low, M., Balsara, D. S., Kim, J., & de Avillez, M. A. 2005, ApJ, 626, 864
McKee, C. F. & Ostriker, J. P. 1977, ApJ, 218, 148
Mohan, R., Dwarakanath, K. S. & Srinivasan, G., 2004, JApA, 25, 143
Stanimirović, S. & Heiles, C., 2005, ApJ, 631, 371
Stanimirović, S., Heiles, C., & Kanekar, N. 2007, SINS - Small Ionized and Neutral Structures in the Diffuse Interstellar Medium, 365, 22
Wolfire, M. G., McKee, C. F., Hollenbach, D., & Tielens, A. G. G. M. 2003, ApJ, 587, 278